4
Comparative Interaction of TCPy and PM with BSA and relative BSA esterase activity

4.1 INTRODUCTION

In recent years studies related to organophosphate pesticides (OP) toxicity have received much attention. However, there is a scarcity in research related to metabolites of these pesticides. It is immensely important to understand the molecular interaction of these OP metabolites with vital biomolecules, especially with the proteins. As discussed in Chapter 3, Chlorpyrifos (CPF) and parathion (PA) are the two most commonly used commercial pesticides which eventually degrade into 3,5,6-trichloro-2-pyridinol (TCPy) and paraoxon methyl (PM) respectively [Dahiya et al, 2017; Racke, 1993; Woodburn et al, 1993; Wu and Linden, 2008]. In this Chapter, the interaction of OP metabolites, TCPy and PM with BSA, are examined by employing *in vitro* ligand-observed ^{1}H NMR experiments, especially ^{1}H spin-lattice relaxation-based experiments besides monitoring of chemical shift changes and saturation transfer difference (STD). The molecular structures of these two metabolites are shown in Figure 1.11 and 1.13. The experimental observation allows the prediction of distribution and fate of these two OP metabolites with plasma protein. Further, to achieve complete information regarding the ligand binding process, both Fluorescence quenching and molecular docking analysis are performed revealing the stoichiometry of the complexes and the various molecular interactions involved in the process of complexation. Figure 4.1 gives a graphical illustration of the experimental methods used to investigate the said OP-BSA interaction. BSA being a multifunctional protein, possesses catalytic properties against a variety of xenobiotic substrate, a property of BSA that is formally known as an enzyme-like or a pseudo-enzymatic activity [Goncharov et al, 2015]. Therefore, this Chapter further tries to analyse the aforementioned property of BSA during the complexation with OP metabolites. A series of hydrolysis study of OP in the presence of BSA has been employed to extract useful information regarding catalytic degradation of these molecules in the presence of BSA [Hansen et al, 2002]. Although, TCPy and PM interaction with serum albumin may not directly indicate their toxicity towards body tissues, but on the other hand, this can help us to predict their behavior with other proteins.

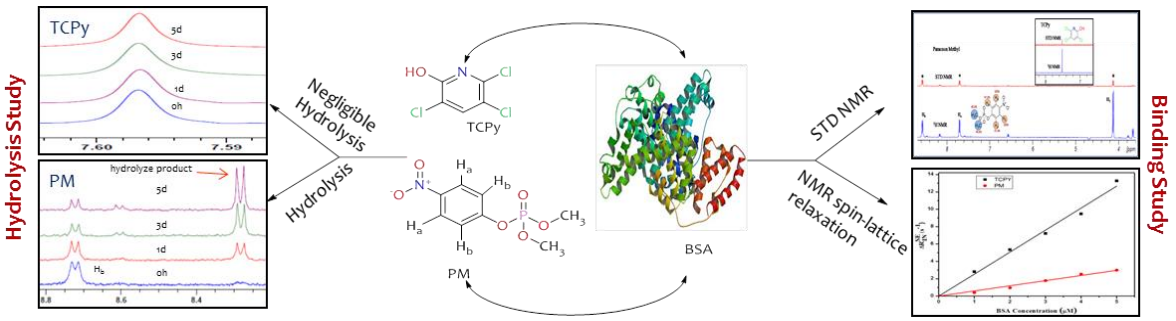

Figure 4.1 : Graphical representation of TCPy-BSA and PM-BSA.

4.2 SAMPLE PREPARATION

The stock solution of BSA was made in deuterated PB (40 mM) at pH 7.4. TCPy and PM stock solutions in deuterated PB were prepared with a solvent combination of 2:3 D_2O: DMSO [Bonechi et al., 2006; Ma et al, 2016b; Martini et al, 2010; Rossi et al, 2001] for NMR measurements. The affinity constant was measured using the fixed concentration of ligands (1 mM) and varying the protein concentration from 1-5 μM, whereas the K_A determination was done by varying the ligand concentration from 1 mM to 5 mM. For affinity index calculation, in all experiments, the ligand concentration was 1 mM, and the protein concentration was varied from 1- 5 μM in steps of 1 μM, whereas the protein concentration was fixed to 5 μM in binding constant calculation with TCPy and PM concentration varied from 1 mM-4 mM.

For fluorescence measurements, the BSA stock solution was prepared by dissolving in phosphate buffer (PB: 0.04 M; pH 7.4). The stock concentrations were determined to be 20 μM for BSA. PM, TCPy, ibuprofen, and warfarin stock solutions were prepared in DMSO. 10% DMSO was used in the final solutions for measurements. An appropriate volume of metabolites with concentration ranging from $0\text{-}10\times10^{-6}$ mol·L^{-1} were added to BSA (1.0×10^{-6} mol·L^{-1}) and mixed at room temperature.

4.3 EXPERIMENTAL DETAILS

4.3.1 NMR Analysis

In the present Chapter, changes in chemical shift positions and peak integrals of the OP metabolites in the presence and absence of BSA have been monitored for preliminary confirmation of binding interaction as well as possible hydrolysis of the OP metabolites over time. It has been found that PM exhibits a significantly higher rate of hydrolysis in the presence of BSA, as discussed in the result section. Although, a set of STD NMR experiments are performed to comment on the group epitope map of both the metabolites, complete quantitation of the complexation process in terms of the binding constants is not possible with STD due to the existing hydrolysis process. Hence, non-selective and selective ^1H spin-lattice relaxation based analysis has been employed for extracting the kinetic parameters of the complexation processes.

The acquisition of the STD NMR experiments was made in a similar fashion, as described in Chapter 3, section 3.3.1. The relevant experimental parameters used to set up the STD experiments in the case of TCPy and PM are tabulated in Table 4.1. The ^1H spin-lattice relaxation rates were measured using the inversion recovery $(180°\text{-}\tau_m\text{-}90°\text{-acquisition})_n$ pulse sequence with the initial 180° pulse being either non-selective or selective. The sequences employed were preceded by solvent presaturation to suppress residual water signal. All the experiments were carried out at two different temperatures *viz*., 300 K and 310 K over a spectral width of 9.00 ppm for various recovery periods ranging from 0-30 s. 32 K data points were collected during the acquisition period with a repetition time of 40 s. A total of 8 scans were collected for each experiment. The selective inversion was achieved by employing a Gauss1.1000 shaped 180° pulse. Relaxation times were extracted by plotting the experimental signal intensities against the recovery period (τ_m). A non-linear least square fitting procedure based on the Levenberg-Marquardt algorithm [Marquardt, 1963] was used to extract the relevant relaxation rates. The maximum experimental error in the relaxation rate measurements was 5% throughout the experiments. The linear regression analysis of the experimental data was used for affinity index calculation. The affinity index was calculated according to a method proposed by Martini et al 2010 [Martini et al, 2010]. Table 4.1 presents all the relevant experimental parameters used in setting up the different NMR experiments.

Table 4.1 : Experimental parameters used in current Chapter.

Experimental parameters	STD NMR parameters	Relaxation parameters
Solvents	7:3 (D_2O:DMSO d_6)	2:3 (D_2O:DMSO d_6)
Temperature	300 K	300 K and 310 K
Number of scans	2048	8
Saturation time	2 s	-
Shaped pulse for saturation	50 ms Gaussian pulses	Gauss1.1000
On-resonance frequency	–3 ppm	-
Off-resonance frequency	30 ppm	-
Spin lock time	30 ms	-
Solvent presaturation	Squa100.1000	Squa100.1000

4.3.2 Fluorescence spectroscopy

Fluorescence emission of BSA was measured by scanning the solutions using a Perkin Elmer, LS 55 fluorescence spectrophotometer in the range of 250-460 nm using a 1.0 cm quartz cuvette. The excitation and emission slit widths were set to 5 nm throughout the experiments with a scanning speed of 300 nm/min. An appropriate volume of metabolites solutions were added to BSA (1.0×10^{-6} mol $\cdot L^{-1}$) that ranged from 0-10×10^{-6} mol $\cdot L^{-1}$ and mixed at room temperature. The excitation wavelength was fixed at 280 nm. All solutions were kept in the refrigerator in a temperature range of 0-4°C. Analytical grade reagents were used for all experiments, and double distilled water was used throughout the experiments. Site-marker competition experiments were conducted with the use of warfarin and ibuprofen, which primarily binds to site I and site II of BSA, respectively.

4.3.3 Molecular Docking

The structure of ligand TCPy and PM (CID23017 and 329757097) were obtained from pub-chem. The ligands were initially prepared for interaction studies using 'prepare ligand wizard' of Discovery studio 4.0 (DS4). X-ray crystal structure of BSA (PDB ID: 4F5S), was obtained from Protein Data Bank (PDB). The experimental details relevant for further preparation are already discussed in Chapter 3 section 3.3.2.

4.4 RESULTS AND DISCUSSION

4.4.1 Hydrolysis of TCPy and PM

An interesting observation of spectral changes in terms of appearance and disappearance of ^1H NMR peaks of OP metabolites has been made as a function of time that has triggered our interest to understand the fate of these OP metabolites in solution in presence and absence of serum albumin. OP metabolites are generally formed via natural degradation of OP pesticides due to various processes that are either hydrolytic or oxidative or chemical or photolytic in nature [Ferri et al, 2015]. The Figure 1.11 and 1.13 given in Chapter 1, exhibits the generation and further degradation of the OP metabolites TCPy and PM into several small products [Bourquin et al, 1979; John and Shaike, 2015]. The degradation of TCPy and PM *via* hydrolysis can be conveniently

followed by monitoring changes in ^{1}H NMR peak intensities that, in addition, also provides valuable information on the possible effect of serum albumin on the degradation process. A preliminary measurement of ^{1}H NMR spectra of TCPy and PM in different solvent systems over time revealed a number of stimulating facts related to the hydrolysis of these molecules in the aqueous medium. Due to sparing solubility of PM in water, the stock solution of PM is prepared in dimethyl sulfoxide (DMSO) while that of TCPy is prepared both in water and in DMSO.

The fraction of hydrolyzed PM is determined as a function of time by the integration of the proton signals assigned to the two breakdown products: diethyl phosphate and 4-nitrophenol (4-NP) [IPCS Inchem, 1992], relative to the corresponding signals from an intact PM molecule. TCPy remained stable for the same time period used for the PM hydrolysis study. During the study of metabolite-BSA interaction, it is observed that PM starts degrading after 8 h in the free form while in the presence of BSA, the rate of degradation is even faster, as shown in Figure 4.2 [Sogorb et al., 2007]. Figure 4.2 exhibits the dependence of the hydrolysis rate of PM on protein concentration measured for the duration of 12 hrs from the time of sample preparation. A close inspection of Figure 4.2 reveals that in the presence of protein with concentration ranging from 1-5 μM the metabolite remained stable over an initial period of 6 hrs. While above 5 μM concentration, the process of degradation in the presence of protein started even earlier. Therefore, the study clearly indicates the possibility of using serum albumin as a detoxifying agent for PM. On the other hand, TCPy does not undergo any degradation in the presence of protein. A complete analysis of the hydrolysis rate of both the metabolites has been presented in the following section. Considering the effect of degradation, all the relaxation measurements are carried out within 6 hrs of sample preparation for both free and complexed metabolites.

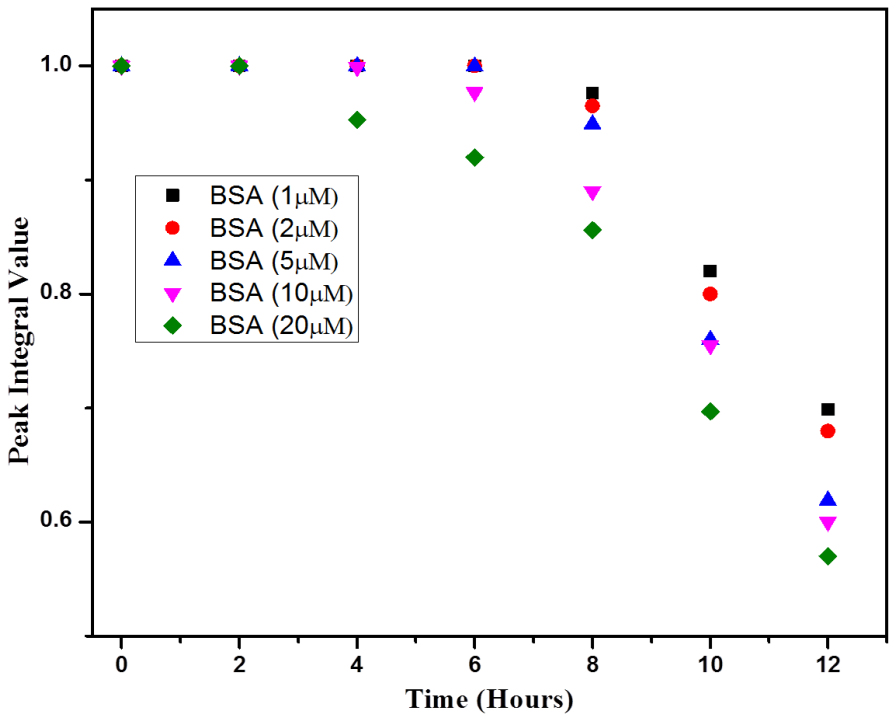

Figure 4.2 : PM degradation study (integration versus time) in D_2O: DMSO (2:3) with increasing BSA concentration. With increasing BSA concentration, the degradation of PM is faster (during 12 hrs).

To quantify the hydrolysis of TCPy and PM in the presence and in absence of protein, three different sets of solutions are used. In the first case, the metabolites are dissolved in 100% DMSO, while in the second and third cases, 3:2 ratio of DMSO: D_2O solutions are used as the

solvent. A maximum of 5 µM of serum albumin is added to the third solution. Finally, the ^{1}H NMR spectra with water presaturation over a total time period of 120 hrs are recorded for all the three solutions to compare the hydrolysis in different solvents conditions for both the metabolites. Figure 4.3 represents the ^{1}H NMR spectra of TCPy recorded in three different solvents for a time period ranging from 0 hr to 120 hrs. It is clearly seen that over a period of 5 days, TCPy remains completely stable in all the solutions. On the other hand, comparison of ^{1}H NMR spectra of PM dissolved in three different solvents revealed that PM is comparably stable in 100% DMSO solvent for a period of 120 hrs as shown in Figure 4.4 while the degradation process for PM is prominent in DMSO: D_2O solvent mixture and becomes even more pronounced in the presence of BSA after an initial period of *ca.* 6 hrs as shown in Figure 4.2. Figure 4.5 shows the degradation of PM protons in the absence and presence of 1 µM BSA.

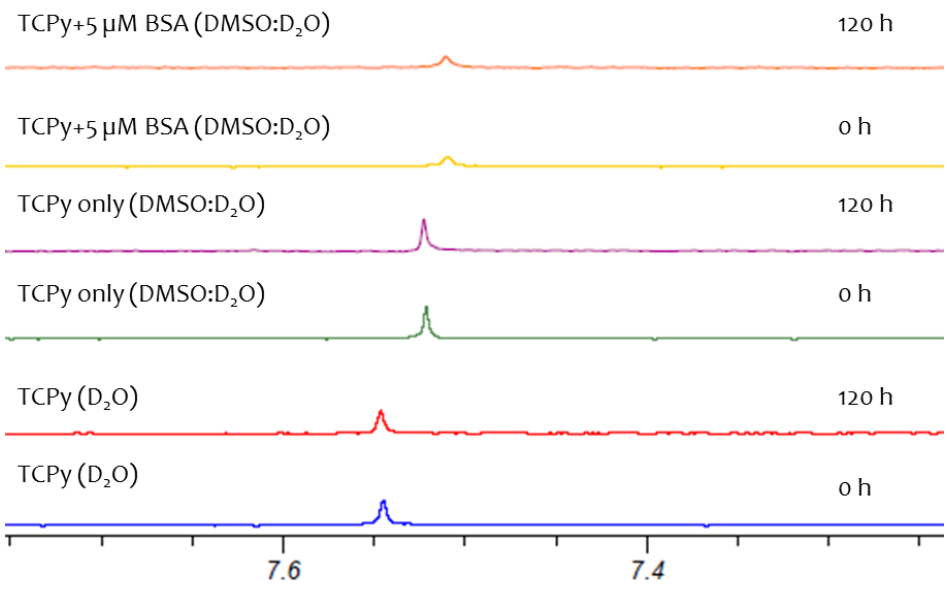

Figure 4.3 : The hydrolysis for TCPy in different solvents in the absence and presence of BSA.

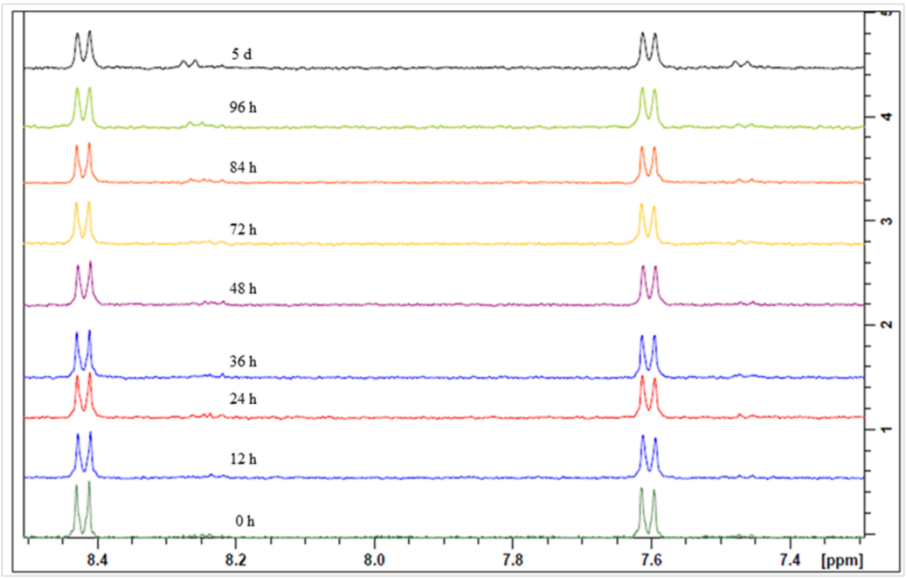

Figure 4.4 : The hydrolysis for PM in the absence of BSA in DMSO. An intensity analysis revealed that PM remains nearly stable in DMSO over a time period of 5 days.

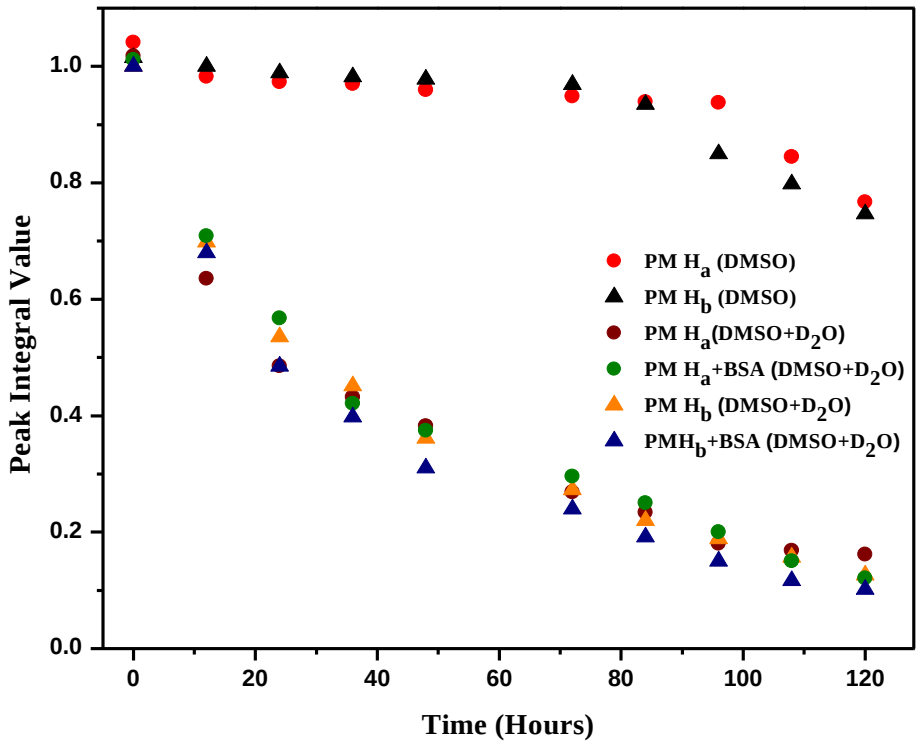

Figure 4.5 : PM degradation study (integration versus time) in DMSO and DMSO: D_2O (3:2). For DMSO: D_2O, both PM free and in bound state with BSA (1 μM), which shows that in the presence of BSA degradation of PM is faster.

The hydrolysis products of PM generated due to P–O bond hydrolysis are identified as *p*-nitrophenol (NP) and dimethyl phosphoric acid by monitoring the disappearance of the aromatic resonances of PM (8.72 ppm and 7.86 ppm) and the appearance of the aromatic resonances at 8.28 ppm and 6.67 ppm for NP in the ^1H NMR spectrum following standard literature values of the chemical shift positions of aromatic protons of PM and NP [Moctezuma et al, 2007]. Figure 4.6 exhibits the general trend of experimentally measured peak integrals of ring protons of PM as a function of time in different solvent conditions. In order to evaluate the hydrolysis rate constant as well as the half-life of the process, the H_b proton integral data extracted for 0- 2 μM BSA concentration are then fitted with Eq.(4.1) and presented in Figure 4.7.

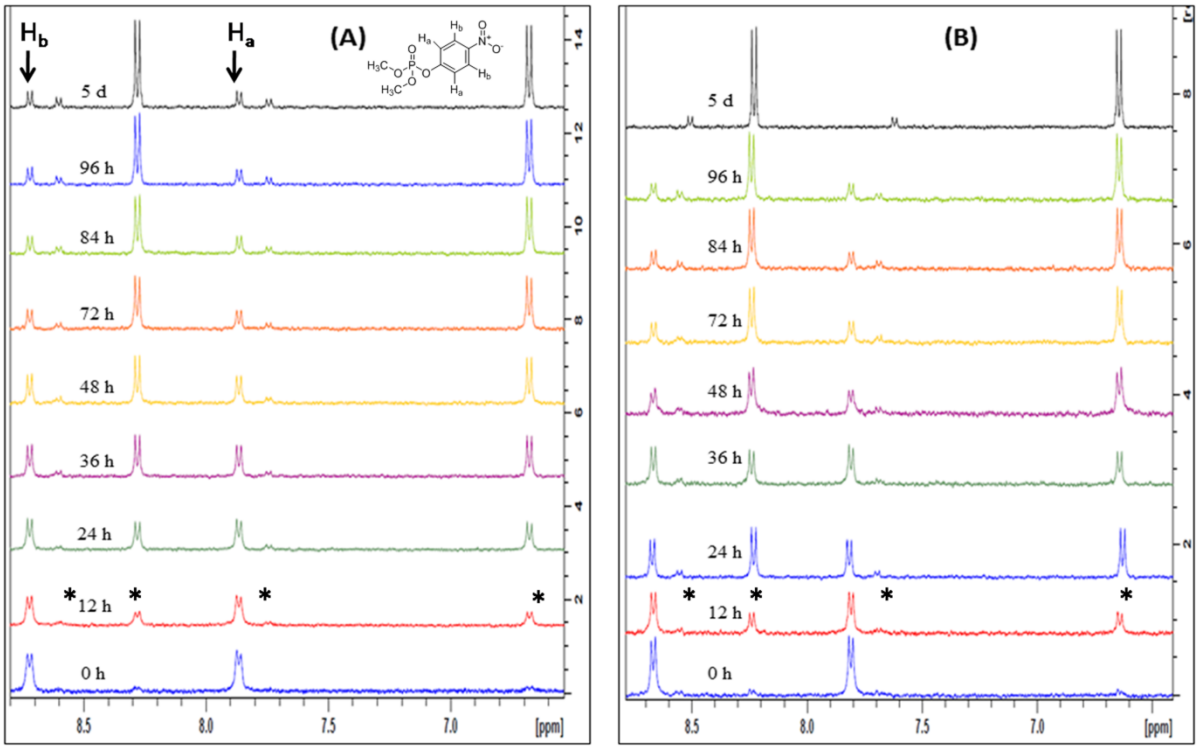

Figure 4.6 : ^{1}H NMR stack plot of the breakdown of PM in to *p*-nitrophenol (NP) at 7.4 pH **(A)** The hydrolysis of PM in absence of BSA and **(B)**The hydrolysis of PM in presence of BSA (1 μM) at different time intervals from 0 hrs, 12 hrs, 24 hrs, 36 hrs, 48 hrs, 72 hrs, 84 hrs, 96 hrs and 5 days at temperature 300 K. t = 0 h, stands for the spectra recorded immediately after dissolving PM. * indicates the peak corresponding to the hydrolysis product with significant intensity.

Eq.(4.1) is used considering the hydrolysis process to be a pseudo-first-order reaction [L'Homme, Arbelot, Puigserver, & Biagini, 2003]:

$$C = C_0 exp(-k_{obsd} t) \quad (4.1)$$

where t is the incubation time in minutes, C is the concentration of PM at time t, C_0 is the initial concentration, and k_{obsd} in min^{-1} is the observed rate constant of the reaction.

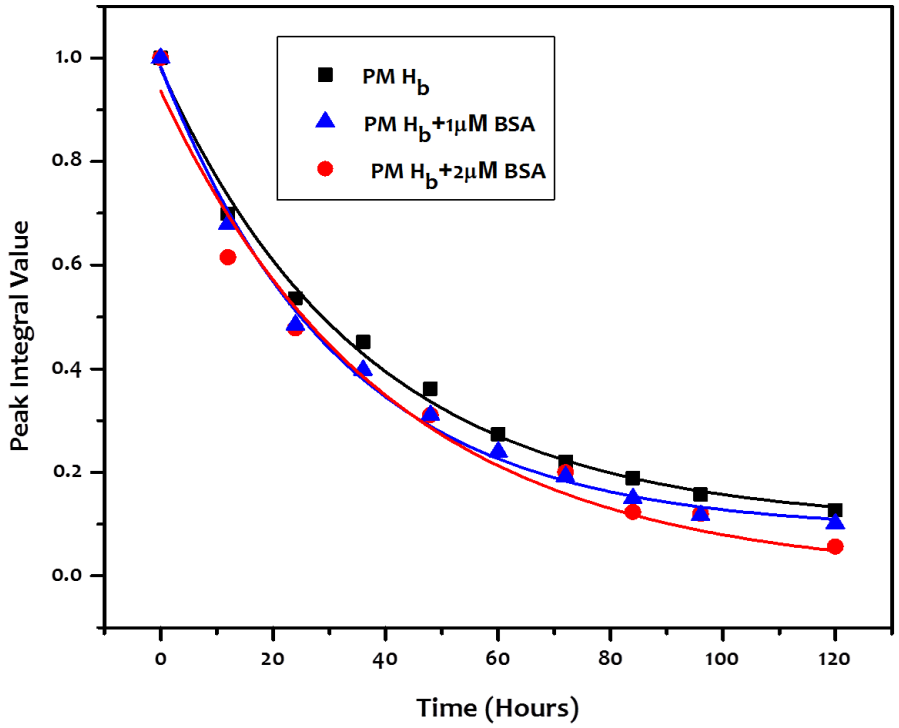

Figure 4.7 : Degradation of PM (H_b) represented as a function of time in the absence of BSA and in the presence of 1 μM BSA and 2 μM BSA at pH 7.4 as determined by ^{1}H NMR analysis.

Table 4.2 summarizes the observed rate constants and half-lives in the absence and presence of BSA at pH 7.4 and 27 °C. A close inspection of Table 4.2 reveals that the hydrolysis rate and the half-life in presence of 1 μM protein is 12% faster compared to that of the pesticide without protein. An increase in hydrolysis rate by *ca.*, 20% is clearly observed for a concentration increase of BSA from 1 to 2 μM signifying molecular interaction of PM with BSA with subsequent degradation. However, BSA did not exhibit a similar effect in the case of TCPy as validated by the ^{1}H NMR spectra of TCPy recorded in the presence and absence of the protein (Figure 4.3).

Table 4.2 : Observed Pseudo-First-Order Disappearance Rate Constant (hydrolysis rate constant) for PM in absence and presence of BSA (1 μM) and half-lives for PM hydrolysis both for free PM and PM bound with BSA.

Compounds	Hydrolysis Rate Constant	Half Life ($t_{1/2}$)	R^2
PM	$(3.6\pm0.15)\times10^{-4}$ min^{-1}	(1925±81.8) min	0.926
PM+BSA (1 μM)	$(4.1\pm0.17)\times10^{-4}$ min^{-1}	(1689±73.6) min	0.985
PM+BSA (2 μM)	$(4.9\pm0.02)\times10^{-4}$ min^{-1}	(1414±7.35) min	0.906

4.4.2 Quantification of ligand-protein interaction

To analyze the ligand-protein interaction, measurement of chemical shift (δ), line width, non-selective (R_1^{NS}), and selective (R_1^{SE}) relaxation rates are carried out at different protein and ligand concentrations for both TCPy and PM. Detailed ^{1}H chemical shift and line width values of TCPy and PM with and without BSA have been summarized in Table 4.3**.** The chemical shift change is due to alteration in the chemical and electronic environment of TCPy and PM in the presence of BSA.

Tables 4.3 : The ^{1}H-NMR chemical shifts of TCPy and PM.

	PM (H_b)		**TCPY**	
	Chemical Shift (ppm)	Line Width (Hz)	Chemical Shift (ppm)	Line Width (Hz)
Without BSA	8.72	2.29	7.52	2.09
With BSA (5 μM)	8.22	3.24	7.51	4.31

4.4.3 STD NMR Experiments

To further confirm the binding event between BSA-TCPy and BSA-PM, saturation transfer difference (STD) experiments are carried out.

shows the STD reference and difference spectra acquired for 400 μM of PM in the presence of 10 μM BSA in 40 mM PB while the same set of spectra for TCPy is presented in the inset. It is evident from the Figure that a significant STD effect is observed in case of both the OP metabolites.

The relative STD values for PM protons are obtained on the basis of peak integral values, which confirm that the H_b proton of PM is in close proximity with BSA than H_a and CH_3 protons. However, similar epitope mapping is not advantageous in the case of TCPy having a single proton. It must be noted here that a complete quantitation of the complexation event employing STD NMR in the present case of PM is not viable due to the prominent hydrolysis process of PM in the presence of BSA. Therefore, a detailed experimental determination of kinetic parameters of the OP metabolite-BSA complexes is presented using spin-lattice relaxation rate measurements.

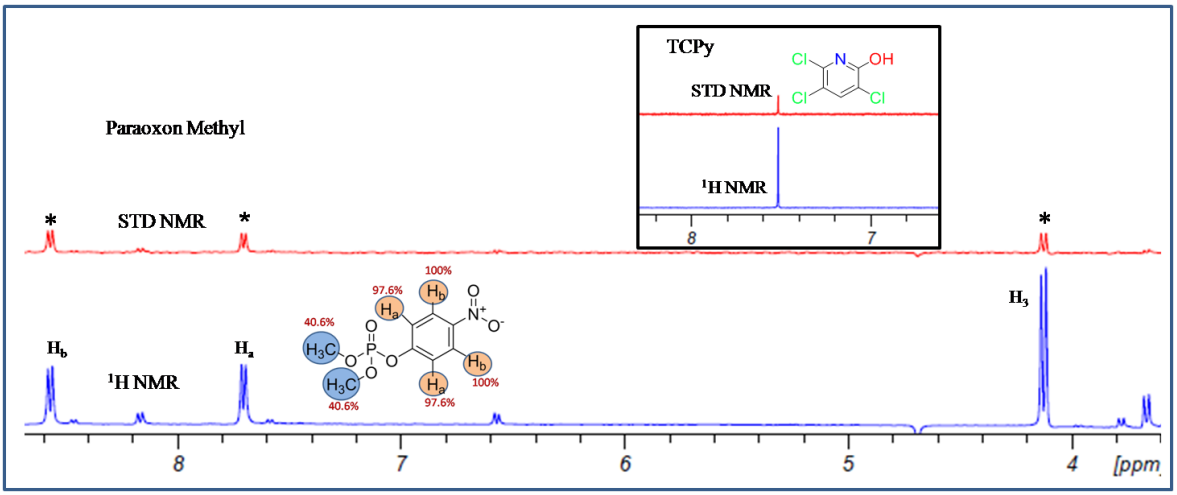

Figure 4.8 : ^{1}H and STD NMR spectra of TCPy (inset) and PM in the presence of BSA. NMR spectra are recorded at 300 K with 2.0 s saturation time, 400 µM concentration of ligand and 1:40 receptor-to-ligand ratio in 40 mM PB (pH = 7.4±0.5), and 30% DMSO-d_6 at 500 MHz.

4.4.4 NMR Relaxation Study

Chapter 2 section 2.3.4 gives a detailed description of non-selective (R_1^{NS}) and selective spin-lattice relaxation rate (R_1^{SE}) measurement used for ligand-protein interaction analysis. In this section non-selective and selective ^{1}H spin-lattice relaxation rates are measured for the OP metabolite protons as a function of both protein and ligand concentration to extract the relevant kinetic parameters of the OP metabolite-BSA complexation. In all the experiments, the range of protein concentrations is used in such a way so that the solution viscosity remains unchanged. To differentiate the genuine ligand-protein interaction over viscosity effect variable temperature non-selective and selective relaxation rate measurements are performed. It is found that with an increase in temperature, the ligand in the presence of protein exhibits reduction in both R_1^{NS} and R_1^{SE} with the condition $R_1^{NS}<R_1^{SE}$ remaining true, which confirms the ligand-protein binding [Martini et al., 2006]. Table 4.4 reveals that both $R_1^{NS}$and R_1^{SE} decrease with the increase in temperature, which confirms that the free metabolites experience the fast motion condition even in the presence of BSA. A representative set of experimental values of R_1^{NS} and $R_1^{SE}$of TCPy and H_b proton of PM with varying BSA concentration has been presented in Table 4.5. In the case of PM, exactly similar values have been obtained for H_a proton while the methyl proton relaxation rates have not been considered as it is also influenced by other relaxation mechanisms besides dipolar interactions. In the absence of BSA, R_1^{NS} has a greater experimental value compared to R_1^{SE} indicating that both OP metabolites are in the fast re-orientational motion regime. On the other hand, in the presence of protein R_1^{SE} becomes larger compared to R_1^{NS} due to slowing down of ligand's dynamics by complex formation with albumin. [Bonechi et al, 2011]. As expected the molecular correlation times (τ_c) measured for both the OP metabolites exhibit a gradual increase in magnitude with the increase in protein concentration as presented in Table 4.5 and confirm the ligand-protein interaction. The r_{ij} value for TCPy is taken as 1.09 Å for C–H bond length, and for PM r_{ij} value is 2.43 Å for H–H bond length [Kasahara et al., 2009,Y. Li et al., 2007,Reddy et al., 2015]. For the bound state, the τ_c is calculated using the ratio of R_1^{SE}/R_1^{NS}.

Tables 4.4 : R_1^{NS} and R_1^{SE} values for TCPy and PM (1 mM) in the absence and presence of BSA (5 μM) at 300 K and 310 K [Rossi et al., 2001].

	TCPy				PM			
BSA (μM)	R_1^{SE}(s^{-1}) (300 K)	R_1^{SE} (s^{-1}) (310 K)	R_1^{NS} (s^{-1}) (300 K)	R_1^{NS} (s^{-1}) (310 K)	R_1^{SE} (s^{-1}) (300 K)	R_1^{SE} (s^{-1}) (310 K)	R_1^{NS} (s^{-1}) (300 K)	R_1^{NS} (s^{-1}) (310 K)
0	0.184 ±0.002	0.161 ±0.006	0.197 ±0.005	0.192 ±0.005	0.218 ±0.002	0.207 ±0.003	0.220 ±0.003	0.214 ±0.002
5	0.342 ±0.004	0.335 ±0.003	0.290 ±0.003	0.264 ±0.004	0.239 ±0.001	0.226 ±0.005	0.227 ±0.004	0.221 ±0.001

Table 4.5 : R_1^{NS} and R_1^{SE} values for TCPy and PM (1mM) in the absence and presence of variable concentration of BSA at 300 K.

	TCPy					PM				
BSA (μM)	R_1^{NS} (s^{-1})	R_1^{SE} (s^{-1})	ΔR_1^{SE} (s^{-1})	ΔR_{1N}^{SE*}	τ_c (s) (300 K)	R_1^{NS} (s^{-1})	R_1^{SE} (s^{-1})	ΔR_1^{SE} (s^{-1})	ΔR_{1N}^{SE*}	τ_c (s) (300 K)
0	0.197 ±0.005	0.184 ±0.002	0	0	(0.87±0.01) ×10^{-11}	0.220 ±0.003	0.218 ±0.002	0	0	(8.01±0.07) ×10^{-11}
1	0.199 ±0.003	0.208 ±0.001	0.024	0.130	(4.2±0.08) ×10^{-10}	0.220 ±0.005	0.219 ±0.002	0.001	0.004	(4.26±0.13) ×10^{-10}
2	0.221 ±0.002	0.250 ±0.003	0.066	0.358	(4.81±0.10) ×10^{-10}	0.219 ±0.002	0.220 ±0.003	0.002	0.009	(3.96±0.09) ×10^{-10}
3	0.281 ±0.001	0.307 ±0.001	0.123	0.668	(4.56±0.03) ×10^{-10}	0.223 ±0.001	0.225 ±0.002	0.007	0.032	(3.93±0.05) ×10^{-10}
4	0.283 ±0.002	0.316 ±0.001	0.132	0.717	(4.72±0.05) ×10^{-10}	0.225 ±0.003	0.236 ±0.005	0.018	0.082	(3.86±0.13) ×10^{-10}
5	0.290 ±0.003	0.342 ±0.004	0.158	0.859	(5.11±0.11) ×10^{-10}	0.227 ±0.004	0.239 ±0.001	0.021	0.09	(4.29±0.09) ×10^{-10}

4.4.5 Calculation of Normalized Affinity index $[A_N]_L^T$ and binding constant (K_a)

To examine the strength of TCPy-BSA and PM-BSA interactions, the normalized affinity indices $[A_N]_L^T$ of the ligand-protein systems are examined. In Figure 4.9, to extract the normalized affinity indices for both OP metabolite-protein systems, the experimental values of ΔR_{1N}^{SE} have been plotted against concentration of BSA and fitted with Eq.(2.24) as given in Chapter 2.

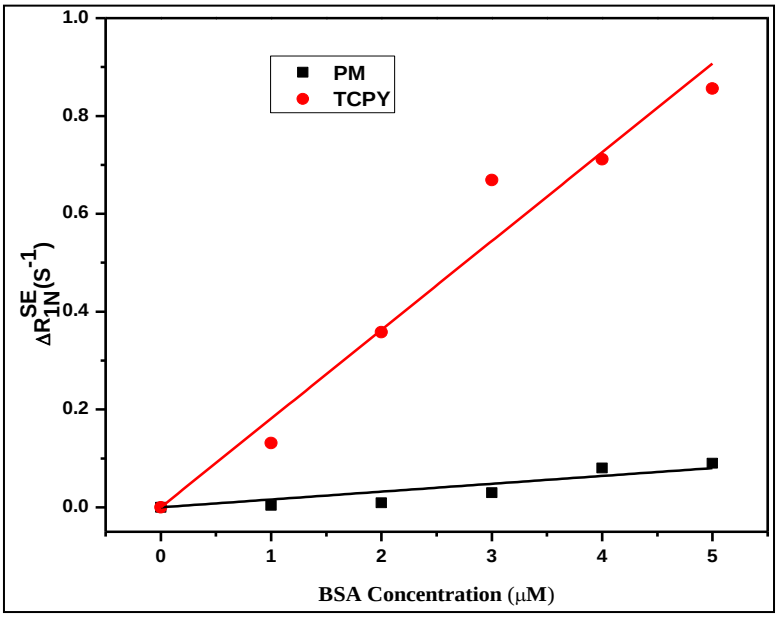

Figure 4.9 : Comparison of the linear regression analysis of TCPy and PM (H_b) by selective relaxation rate enhancement of TCPy and PM against BSA concentration to calculate "normalized Affinity index"$[A_N]_L^T$.

The normalized affinity indices for both the metabolites have been reported in Table 4.6. A close inspection of the values reveals that TCPy has *ca*. eleven times stronger affinity towards BSA compared to PM. This indicates that the structure plays an important role in binding affinity, as discussed in Chapter 3 for the parent OP. Structural comparison of TCPy and PM reveal that TCPy possesses three chlorine atoms yielding a high possibility of halogen bonding with the protein [Liu et al, 2014; Šmejkalová et al, 2009] giving rise to superior binding affinity. The relevance of halogen bonding in biological systems is well known in the literature that documents halogen-bonding between a halogenated ligand and protein backbone and side-chain having Lewis base like character [67]. Halogen contains an anisotropic charge distribution with an equatorial negative charge on one region and a positive electrostatic potential on the outer region (σ-hole), leading to halogen bonding. In literature, it is well reported that ligands with halogen atoms exhibit stronger affinity towards proteins via such halogen bonding [Lin and Mackerell, 2017; Shinada et al, 2019; Wilcken et al, 2013]. Moreover, a comparison of the normalized affinity indices with that of vine pesticides-BSA interaction [Martini et al, 2010] unveiled that both TCPy and PM exhibit an extremely strong binding interaction. Consequently, the bio-availability and the distribution of the OP metabolites are going to be very different compared to that of the vine pesticides reported previously.

To analyze the stability of the complexes, R_1^{SE} for both TCPy-BSA and PM-BSA are measured at two different temperatures with varying metabolite concentrations keeping the protein concentration fixed at 5 μM. The experimental values of $1/\Delta R_1^{SE}$ are then plotted against metabolite concentration, as depicted in Figure 4.10 (a) and (b) for TCPy and PM, respectively. The binding constant is calculated from the intercept while the relaxation rate of the bound ligand is extracted from the slope of the plot following Eq.(2.23). In the case of PM, with the increase in ligand concentration, the change in $1/\Delta R_1^{SE}$ value at 300 K and 310 K is almost insignificant. One may reason out this observation by stating that with higher metabolite concentration, the rate of hydrolysis of PM increases that affects the relaxation rate while higher temperature accentuates the hydrolysis process as well [Bonechi et al, 1996].

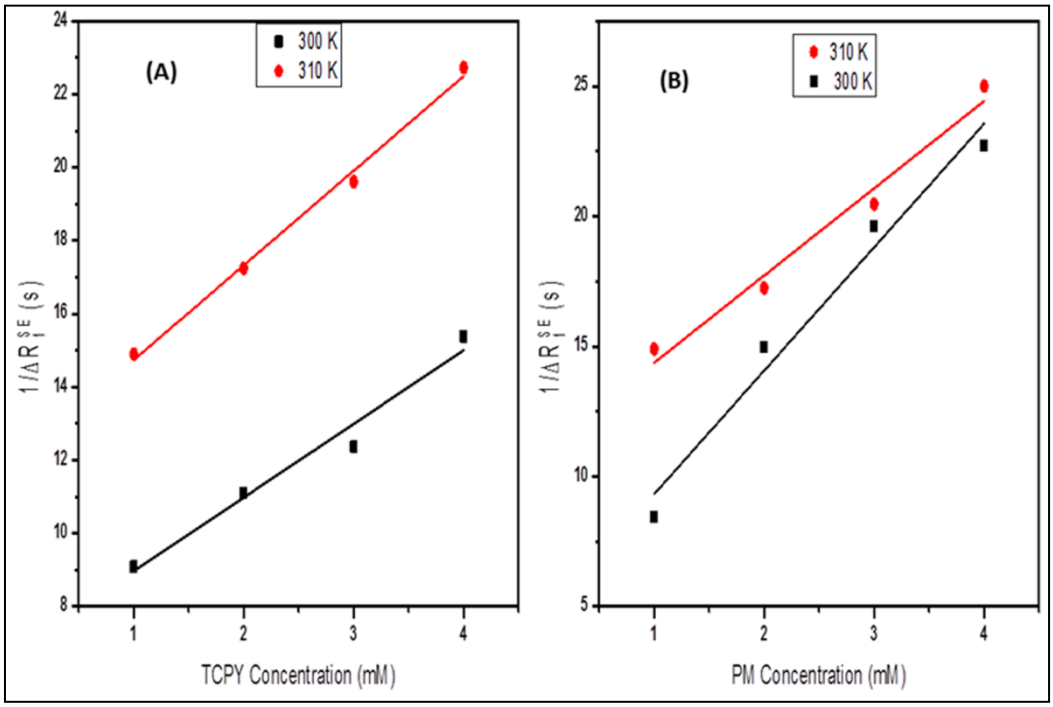

Figure 4.10 : (a) Plot of $1/\Delta R_1^{SE}$ versus TCPy and **(b)** Plot of $1/\Delta R_1^{SE}$ versus PM (H_b) concentration both are ranging from 1 mM to 4 mM with fixed protein concentration 5 µM for binding constant (K_A) calculation.

The parameters thus calculated have been tabulated in Table 4.6, which reveal the relaxation rates of the bound ligands (R_{1B}^{SE}) of the ligand-protein complex at different temperatures. Moreover, the lower R_{1B}^{SE} values of PM at both the temperatures compared to TCPy once again confirm the weaker nature of the PM-BSA complex. As expected, the equilibrium constants for the two metabolites-BSA complexes also follow the same trend with TCPy-BSA showing a 3.5 times greater binding constant at 300 K while 1.4 times greater binding constant at 310 K compared to PM-BSA.

Table 4.6 : Normalized Affinity Index $[A_N]_L^T$; R_{1B}^{SE} and equilibrium constant (K_A=1/K_D) for interaction of BSA and TCPy at different temperatures (300 K and 310 K).

Compounds	$[A_N]_L^T$ **(10^3) M^{-1}**	R_{1B}^{SE}**(300 K) s^{-1}**	R_{1B}^{SE}**(310 K) s^{-1}**	**K_a (300K) L mol^{-1}**	**K_a (310K) L mol^{-1}**
TCPy	181.46±8.72	99.37±8.4	77.34±14.9	3456±27.38	4700±27.47
PM	16.04±2.23	42.15±3.7	59.64±5.7	965±21.74	3286±21.8
R^2	0.986	0.989	0.988	0.989	0.988

Table 4.7 presents all the relevant thermodynamic parameters for both TCPy-BSA and PM-BSA that are evaluated from the binding constants measured at two different temperatures. Analysis of Table 4.7 reveals that for both systems the change in Gibb's free energy shows negative value whereas the change in enthalpy and the change in entropy show positive values. According to the views of Ross and Subramanian (1981) [Ross & Subramanian, 1981], the negative ΔG values suggest that the binding interactions are spontaneous, whereas the positive ΔH values show that the formation of complexes are endothermic. The positive values of ΔH and ΔS obtained for the interaction between metabolites and BSA reveal that hydrophobic interaction plays an important role in stabilizing the complexes [Zhang et al, 2007]. Further, the magnitude of ΔG value determines the stability of the ligand-protein complex or binding affinity of the given ligand to the protein, which confirms that the binding of TCPy is stronger than PM [Du et al, 2016]. These results support that the affinity index analysis for TCPy indicating TCPy as a better binder than PM is valid. The extraction of thermodynamic parameters has been limited to two temperature analyses to complete the variable-temperature measurement within a total experimental time period of 6 hrs to avoid initiation of PM degradation. Further, the temperature range is kept up to 310 K as PM hydrolysis becomes faster at higher temperature causing experimental determination of relaxation rate ambiguous.

Table 4.7 : Thermodynamic parameters for TCPy-BSA and PM-BSA interaction.

Compounds	ΔG (kJ mol^{-1})	ΔH (kJ mol^{-1})	Δ S (J $mol^{-1}K^{-1}$)
TCPy	-20.32	23.77	146.98
PM	-17.14	94.74	372.93

4.4.6 Molecular Docking

Insilco docking studies are further carried out for a better understanding of the *in vitro* interaction of these pesticide molecules with BSA besides validating the experimentally obtained NMR and fluorescence data. The molecular docking data clearly indicates the strong interaction of TCPy and PM with BSA. It is well known that the BSA monomeric structure has two binding sites Site I and Site II and three hydrophobic subdomains I, IIA, and IIIA, respectively [Wang et al, 2016]. The observed results are shown in Figure 4.11 highlight the binding microenvironment of TCPy. The molecule is surrounded by two hydrophobic residues PRO117, LYS114. It forms two electrostatic bonds with amino acid residues LYS114, ARG185, and one hydrogen bond with LYS114 residue with Cdocker interaction energy of -17.99 kcal/mole in the subdomain site I, and IIA of BSA. These docking results stated that the hydrophobic and electrostatic interactions with hydrogen bond promote TCPy-BSA interaction.

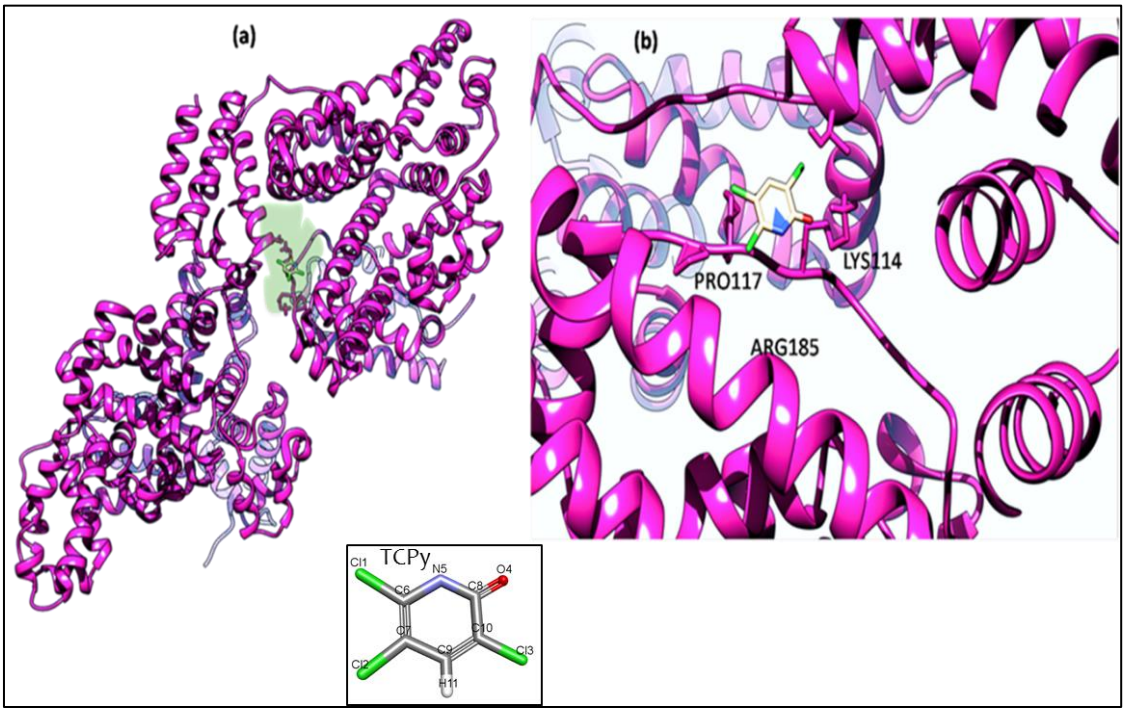

Figure 4.11 : Interaction of TCPy with the BSA (PBD ID 4F5S): **(a)** The green coloured highlighted region is the Site of Interaction. **(b)** displays a snap shot of BSA-TCPy complex with its respective interacting residues.

Similarly, the docked complex of PM with BSA shown in Figure 4.12 actively interacts through hydrogen bonding with three amino acid residues ARG185, LYS114, THR518. Moreover, LYS116, PRO516, LYS114, ARG185 are involved in hydrophobic interaction and ARG185, GLU182 in electrostatic interactions in to subdomain IIA and IIIA with Cdocker interaction energy of -31.89 kcal/mole. It should be noted here that the measured Cdocker interaction energy for PM shows a higher negative value compared to that of TCPy, indicating PM being a better binder to BSA. This clearly contradicts the previous experimental findings. However, it must be considered that during the docking process, the halogen bonding interaction in the case of TCPy has not been taken in to account. On top of it, the experimental condition of hydrolysis for PM has also not been considered during the docking study. These two reasons could definitely lead to an overestimation of CDocker interaction energy in the case of PM. It is necessary to point out that molecular docking studies in case of TCPy and PM have been performed to get an overall qualitative idea of binding modes.

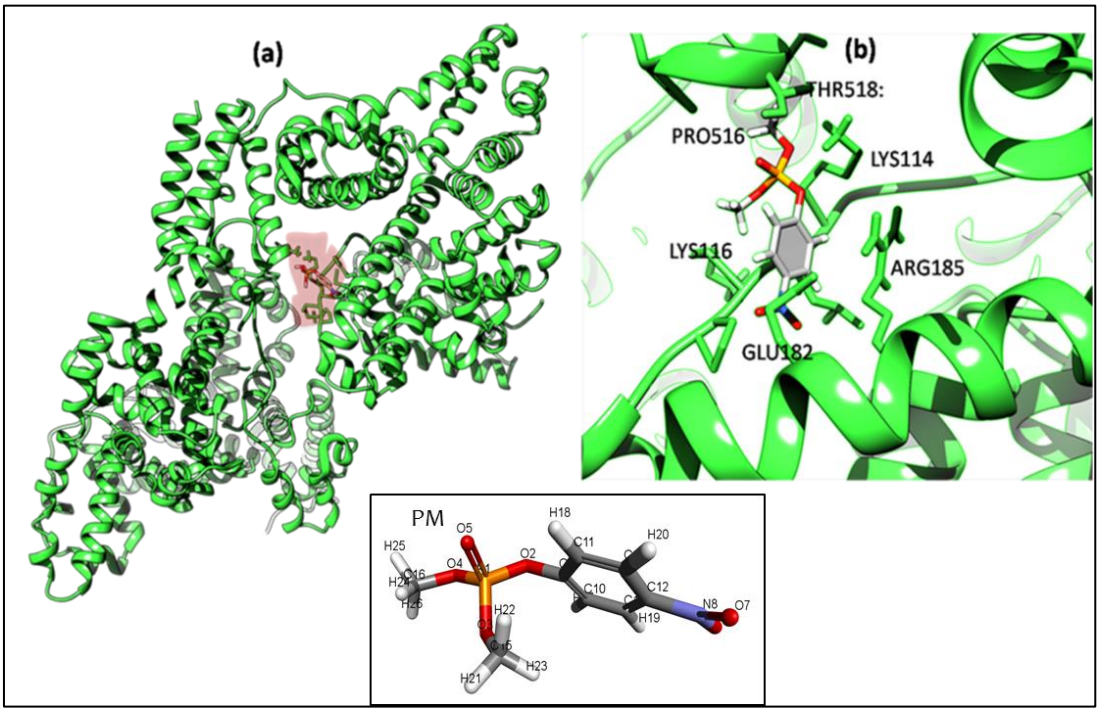

Figure 4.12 : Interaction of PM with the BSA (PBD ID 4F5S): **(a)** The red coloured highlighted region is the Site of Interaction. **(b)** displays a snap shot of BSA-PM complex with its respective interacting residues.

From this data it is evident that hydrogen bonding, hydrophobic interaction, and electrostatic interaction play a major role in triggering active and strong interaction between BSA and metabolite complexes, as given in Table 4.8 and 4.9 [Liu et al, 2018]. These results are in favor of findings from the thermodynamic study.

Table 4.8 : Summary of interactions between TCPy-BSA

Interacting Residues	Bond Length (Å)	Interaction Type
TCPY:N5B:ARG185:NH1	4.5	Electrostatic
TCPY:Cl2 - B:PRO117	5.0	Hydrophobic
TCPY - B:LYS114	5.1	Hydrophobic
TCPY:N5B:LYS114:NZ	5.0	Electrostatic
TCPY:O4B:LYS114:HZ1 -	1.8	Hydrogen Bond

Table 4.9 : Summary of interactions between PM-BSA

Interacting Residues	Bond Length (Å)	Interaction Type
PM:O6 B:ARG185:HD2	2.9	Hydrogen bond
PM:C15 - B:LYS116	4.6	Hydrophobic
PM:O4B:LYS114:HZ1 -	1.8	Hydrogen Bond
PM:C16 - B:PRO516	4.6	Hydrophobic
PM:O5B:THR518:HB -	2.5	Hydrogen Bond
PM:C16 - B:LYS114	4.1	Hydrophobic
PM:O6B:ARG185:NH1	5.5	Electrostatic
PM:N8 - B:GLU182:OE2	5.3	Electrostatic
PMB:ARG185:NH1	4.3	Electrostatic

4.4.7. Fluorescence Quenching Mechanism

In this section, a set of fluorescence quenching analysis has been reported as supporting experimental data for the NMR relaxation analysis. Further, site marker fluorescence quenching experiments are performed to identify the BSA binding sites accessed by the OP metabolites. As shown in Figure 4.13 fluorescence intensity of BSA gradually decreased with increasing concentration of both metabolites with a fixed concentration of BSA confirming the interaction of the BSA-OP metabolites [Dahiya et al, 2017; Ma et al, 2016a].

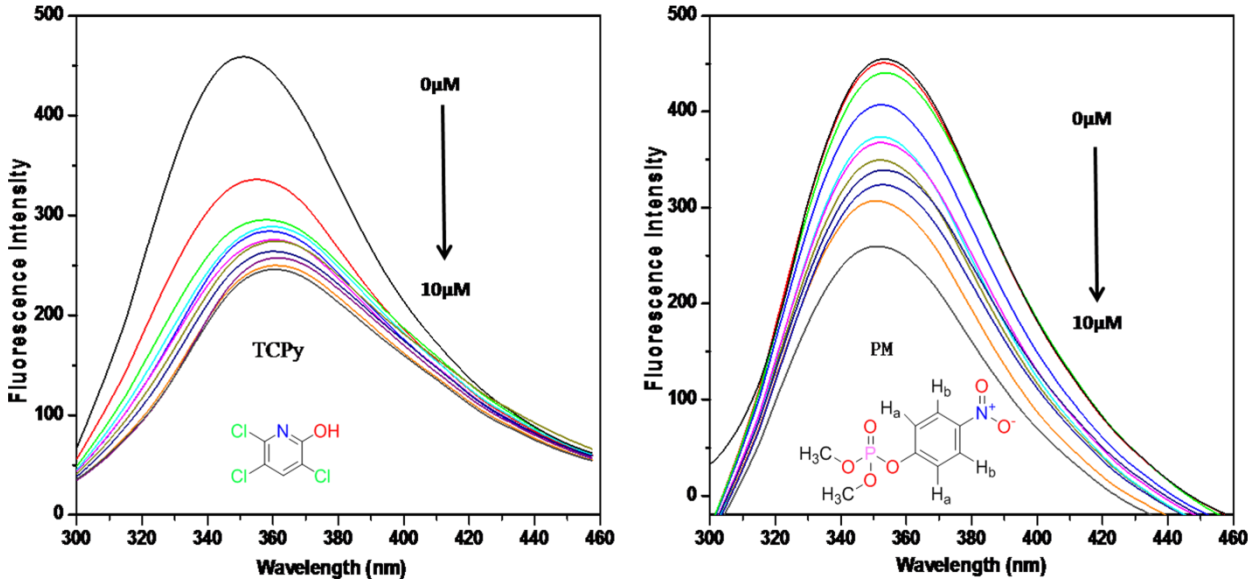

Figure 4.13 : Fluorescence spectra of BSA in the presence of various concentrations of **(a)**TCPy; **(b)** PM. BSA=1.0×10^{-6}mol L^{-1}, TCPy=PM=0-10^{-6}mol L^{-1}, λ_{ex}=280 nm, pH=7.4, room temperature.

As described in Chapter 2, the Stern-Volmer equation [Eftink, 1991,Joseph R. Lakowicz, 2006], as given in Eq.(2.25), is used to examine the quenching mechanism by analyzing fluorescence data for both the metabolites at room temperature. Table 4.10 summarizes all the relevant data**.** Closer inspections of the quenching constants clearly indicate that both the metabolites exhibit static quenching and forms ground state complex with BSA. The Stern-Volmer constant confirms that TCPy shows a high affinity to BSA than PM, confirming the NMR analysis reported in the previous section [Dahiya et al, 2019] .

Further to understand the binding site of these OP metabolites, a set of fluorescence quenching experiments in presence of BSA site markers *viz.,* warfarin for the site I, and ibuprofen for site II are performed (Figure 4.14). It is concluded from the fluorescence site marker competition experiment that both TCPy and PM bind to site I of BSA.

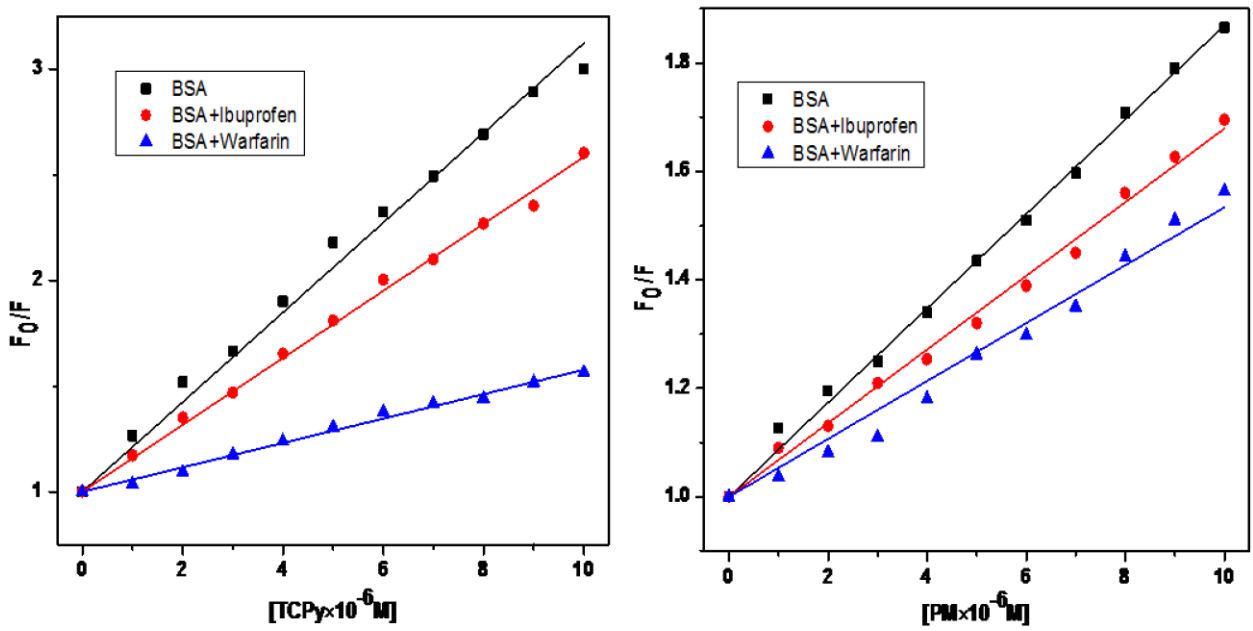

Figure 4.14 : Competition of **(a)** TCPY and **(b)** PM with warfarin and ibuprofen with BSA fluorescence quenching. BSA=Warfarin=Ibuprofen=1.0×10^{-6} mol L^{-1}, TCPY=PM=0-10^{-6} mol L^{-1}, λ_{ex}=280 nm, pH=7.4, room temperature.

The quenching constant in the presence of site marker is determined for both metabolites. The results illustrated in Table 4.8 show that in the presence of warfarin, significant changes are observed for both the metabolites, whereas in presence of ibuprofen, changes are trivial confirming that both the metabolites bind to Site I.

Table 4.10 : Stern-Volmer constant and the quenching constant of BSA with TCPY and PM in absence and presence of site markers.

System	Site-Marker	K_{sv}(L mol^{-1})	K_q(L mol^{-1} s^{-1})	R^2
TCPy-BSA	Blank	2.1×10^5±0.035	2.1×10^{13}±0.035	0.998
	Warfarin	5.7×10^4±0.019	5.7×10^{12}±0.019	0.991
	Ibuprofen	1.5×10^5±0.016	1.5×10^{13}±0.016	0.995
PM-BSA	Blank	4.09×10^4±0.029	4.09×10^{12}±0.029	0.989
	warfarin	2.7×10^4±0.015	2.7×10^{12}±0.015	0.983
	Ibuprofen	3.3×10^4±0.026	3.3×10^{12}±0.026	0.992

4.5 CONCLUSIONS

In this Chapter, complete quantitation of OP metabolite-BSA complexes has been accomplished by employing NMR non-selective and selective ^{1}H spin-lattice relaxation rate measurements. *In vitro* ^{1}H NMR relaxation measurements exemplify a powerful tool to decipher such interaction processes in solution state while time-dependent study of ^{1}H NMR peak intensity change in presence and absence of protein gives valuable information about the stability of OP metabolites. In the present case, ^{1}H NMR spectra of these metabolites recorded as a function of time reveal that TCPy remained stable in the solution in the presence of BSA while PM degradation is accelerated in the presence of BSA. Our results in terms of the non-selective and

selective spin-lattice relaxation rates point out that TCPy is a better binder to BSA, resulting in a more stable complex with the serum albumin with an affinity constant *ca.* eleven times greater than PM due to halogen bonding present in case of TCPy. Consequently, the BSA-TCPy complexation prevents the hydrolysis of TCPy, and the complex behaves like a reservoir for TCPy in serum. On the other hand, PM with a much smaller affinity constant is not only prone to metabolism due to its higher free concentration but also has a greater chance to diffuse to other body tissues [Mourik and Jong, 1978]. Further, these results demonstrate that the structure of a compound play a major role in deciding the interaction with serum albumin. Acceleration of degradation rate of PM in the presence of BSA indicates a catalyzing effect of BSA that allows it to function as a degradation promoter. Hence, the protein can act as a scavenger for PM, preventing other proteins from undergoing covalent alterations due to interaction with the said OP. Although compared to TCPy, PM engenders a greater risk to humans and other organisms [Silva et al, 2004; Wang et al, 2005] due to its higher free concentration in the serum, it has a greater chance to get metabolized by BSA in its free state. A complementary set of data consisting of NMR saturation transfer difference, fluorescence quenching, and molecular docking enabled us to confirm the formation of metabolite-BSA complex and its binding interaction with certainty. The quenching data clearly indicated static binding of these metabolites with BSA Site I involving hydrogen bonding, electrostatic interaction, and hydrophobic interaction as major interaction forces as revealed by molecular docking. Hence, current findings will be helpful in the understanding of the mechanism of toxicity of OP metabolites.

To the best of our knowledge, the present OP metabolites-BSA interaction is reported for the first time. This study will be of particular interest in the ecotoxicology of OP metabolites and environmental risk assessment [Walker, 1998]. The enzymatic properties of BSA can be helpful in designing new biocatalysts that can operate in a waste-free and environmentally acceptable way. The detailed information regarding the degradation pathway of OP will provide therapeutic insights for designing new drugs against OP poisoning.

...